

Service load response prediction of reinforced concrete flexural members

Feng Ning[†], Neil C. Mickleborough[‡] and Chun-Man Chan^{‡†}

Department of Civil Engineering, Hong Kong University of Science & Technology, Kowloon, Hong Kong

Abstract: A reliable and accurate method has been developed to predict the flexural deformation response of structural concrete members subject to service load. The method that has been developed relates the extent of concrete cracking, measured as a function of the magnitude of applied moment in a member, to the reduction in the effective moment of inertia of cracked reinforced concrete members under service load conditions. The ratio of the area of the moment diagram where the moment exceeds the cracking moment, to the total area of the moment diagram for any loading, provides the basis for the calculation of the effective moment of inertia. This ratio also represents mathematically a probability of crack occurrence. Verification of this method for the determination of the effective moment of inertia has been achieved from an experimental test program, and has included beam tests with different loading configurations, and shear wall tests subjected to a range of vertical and lateral load levels. Further verification of this method has been made with reference to the experimental investigation of other recently published work.

Key words: probability; flexural members; deflection; curvature; stiffness; serviceability prediction; moment of inertia; cracking; reinforced concrete.

1. Introduction

The behaviour and response of reinforced concrete at service loads is a necessary consideration in the design process. The methods to determine service load behaviour and adopted by building codes generally, specify the procedure for determining the effective moment of inertia, I_e . The numerical value of I_e lies between the fully cracked and the un-cracked gross moments of inertia ($I_{cr} \leq I_e \leq I_g$). The empirical relationship for I_e , proposed by Branson (1977), has formed the basis and has been adopted in its original or modified form in many codes of practice and specifications for reinforced concrete structures, such as the ACI Building Code (ACI-318 1995), CAN3-A23.3-M84 (CAN 1984) and AS 3600-1994. Eq. (1) represents the general form of the relationship:

$$I_e = \xi I_{cr} + [1 - \xi] I_g \quad (1)$$

where

[†] Research Associate
[‡] Associate Professor
^{‡†} Assistant Professor

$$\xi = \left[1 - \left(\frac{M_{cr}}{M_a} \right)^m \right]$$

M_{cr} and M_a represent respectively the cracking moment and the maximum applied moment on a relevant flexural member and the power coefficient m is taken as 3. ξ represents an interpolation function which considers the effects of cracking and hence the form of loading. Murashev's expression (Murashev 1940) determined that

$$\xi = \left[1 - \frac{2}{3} \left(\frac{M_{cr}}{M_a} \right)^2 \right] \leq 1.0 \quad (2)$$

but the more general form of the interpolation value for ξ , is given by

$$\xi = \left[1 - \beta \left(\frac{M_{cr}}{M_a} \right)^m \right] \quad (3)$$

Experimentally determined values of m have shown varying results from about $m = 2$ to a value as high as $m = 4$. Concentrated loads tend to indicate a larger value of m , $m = 3$ has generally been used for uniformly distributed loading cases.

The CEB-FIP Model Code 1995 (CEB-FIP 1995) presented a model to account for tension stiffening effect when determining the deflections of a cracked member, as represented in Eq. (4).

$$\psi_m = (1 - \xi)\psi_1 + \xi\psi_2 \quad (4)$$

where $\psi_1 = (M/E_c I_g)$ = the curvature of an uncracked gross section; $\psi_2 = (M/E_c I_{cr})$ = the curvature at a cracked section. The mean value for curvature, ψ_m , lies numerically between the two conditions of cracked and uncracked values. For CEB-FIP, the interpolation function accounts for the tension stiffening effect and takes the form of

$$\xi = 1 - \beta \left(\frac{M_{cr}}{M_a} \right)^2 \quad \text{for } M_a \geq M_{cr} \quad (5)$$

in which M_a is the bending moment at the section considered; and $\beta = \beta_1 \beta_2$, where β_1 is the coefficient characterizing the bond quality of the reinforcing bars; $\beta_1 = 1.0$ for high bond bars and 0.5 for smooth bars. β_2 is the coefficient representing the influence of the duration, or of repetition of loading. In most practical applications $\beta_1 = 1$, $\beta_2 = 0.5$, and hence $\beta = 0.5$. The interpolation function Eq. (5) adopts the same form of the second-degree ($m = 2$) function as Murashev's expression with the constant coefficient of 1/2. This approach takes into consideration the breakdown of the tension stiffening effect under long-term or cyclic loading, and also allows for the reduction of the tension stiffening effect when plain bars are used.

Ghali (1993) has shown that both ACI and CEB-FIP methods give accurate predictions of the immediate deflection for uniformly loaded simple beams. The deflection due to a concentrated load is overestimated when the ACI relationship is used whilst the CEB-FIP formulations tend to be more accurate. Ghali has also indicated that the use of I_e according to ACI and Canadian Codes can produce a sizable error, particularly when the reinforcement ratio ρ is small and the ratio M_a/M_{cr} is close to 1. The magnitude of the error appears largely dependent on the shape of the M-diagram for applied loading. This work leads to the conclusion that it may therefore be possible to determine a

relationship for I_e that is a function of the particular shape of the M-diagram. Such an equation may not be accurate for all moment shapes (e.g., when M is constant) or when the reinforcement ratio is variable.

A model has been proposed by Al-Zaid (Al-Zaid *et al.* 1991 and Al-Shaikh *et al.* 1993) to account for the effect of the load type. The variations in the cracked length L_{cr} , defined as the length of the beam segment over which the working moment exceeds the cracking moment M_{cr} , and the effect of the reinforcement ratio were considered in this model. This procedure forms a rational approach to consider some variables that effect the value I_e .

The effect of cracking on the behavior of a flexural member is largely dependent, however, upon the shape of the moment diagram, which in turn is related to the type and form of applied loading. Present practice generally only considers the relationship between variations of stiffness or curvatures and the ratio of M_{cr}/M_a for the determination of section properties in deflection calculations. A rational approach is presented in this paper to determine the value for the power of m , and forms of the interpolation function.

2. Analytical considerations

There are many factors that influence the short-term deflection of a flexural member. These factors include the span length and end constraints, magnitude and distribution of load, material and sectional properties, ratio of reinforcement, and the amount and extent of member cracking. The moment ratio M_{cr}/M_a at any point, or as a function along the member, is a definable variable that can assist in improving the predictive techniques of code equations. Such a variable can also enhance the applicability of predictive formulations to more realistically complex situations.

The work presented aims to establish more accurate relationships between the variation of effective moment of inertia of cracked reinforced concrete members as well as the factors that are important to member response for generally applicable loading conditions. The main effect on the reduction of the stiffness of the flexural members in the serviceability range considered in this study is the loading type effect during cracking. This effect is believed to be one of the dominant factors controlling the cracking behavior of flexural members.

2.1 Mathematical expectation of cracking effects

The effect of cracking on a flexural member is indicated in Fig. 1. With flexural bending, a section is found to crack when the extreme tensile fibre of the section reaches the value of the modulus of rupture of concrete. In other words, a section is deemed to crack when the applied moment is greater than or equal to the cracked moment M_{cr} , which can be obtained as:

$$M_{cr} = \frac{(\sigma_v + f_r) I_{uncr}}{y_t} \quad (6)$$

where f_r = modulus of rupture of concrete = $0.6 \sqrt{f'_c}$ MPa,
 σ_v = axial compressive stress, especially for beam case, $\sigma_v = 0$
 y_t = distance from centroid of gross section to extreme fiber in tension,
 I_{uncr} = uncracked moment of inertia of section

For the regions where $M < M_{cr}$, the concrete is uncracked and is expected to have uncracked

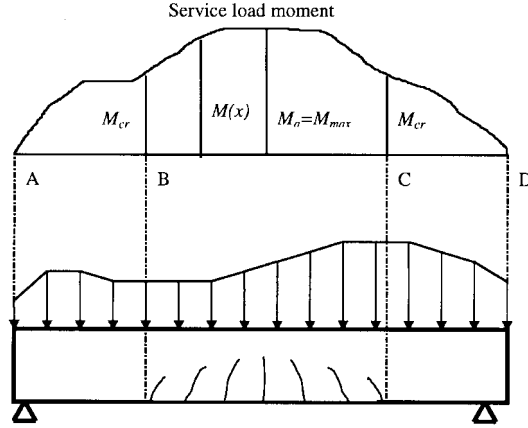


Fig. 1 Various cracking in a reinforced concrete beam carrying service load

section properties. Once flexural tensile cracks develop in the tensile fibres of cracked sections, they propagate gradually towards the neutral axis and reduce the effectiveness of concrete in resisting flexural stresses. As a result, the moment of inertia of the cracked section should then be reduced to the value I_{cr} . The occurrence of cracking is dependent on the shape and magnitude of the moment diagram due to the external load, the larger this magnitude at any location the greater the probability of crack formation.

Consider the location x along a flexural member as an independent random variable. For a flexural member, the outcome of a section cracking or not cracking is directly dependent on the value of the moment on the section, the moment $M(x)$ can thus be regarded as a quantitative measure of the probability distribution of cracking or not cracking over the length of the member. In mathematical terms, the probability distribution (or density) function corresponding to the event of cracking and not cracking can be expressed as

$$p(x) = \frac{M(x)}{S} \quad (7)$$

where $S = \int_0^L M(x) dx$ = total area under the moment diagram. To satisfy the axioms of probability theory, Eq. (7) fulfills the following conditions that $p(x) \geq 0$ and $\int_0^L p(x) dx = 1$.

From the probability distribution function Eq. (7), the probability of having cracks over the region where $M(x) < M_{cr}$ can then be expressed as

$$P_{cr} = P[M(x) \geq M_{cr}] = \int_{\substack{\forall x \text{ such that} \\ M(x) \geq M_{cr}}} \frac{M(x)}{S} dx = \frac{S_{cr}}{S} \quad (8)$$

where $M(x)$ = the moment distribution function and S_{cr} = the area of moment diagram segment over which the moment exceeds the cracking moment. Similarly, the probability of having the moment value less than M_{cr} is

$$P_{uncr} = P[M(x) < M_{cr}] = \int_{\substack{\forall x \text{ such that} \\ M(x) < M_{cr}}} \frac{M(x)}{S} dx = 1 - \int_{\substack{\forall x \text{ such that} \\ M(x) \geq M_{cr}}} \frac{M(x)}{S} dx = 1 - P[M(x) \geq M_{cr}]. \quad (9)$$

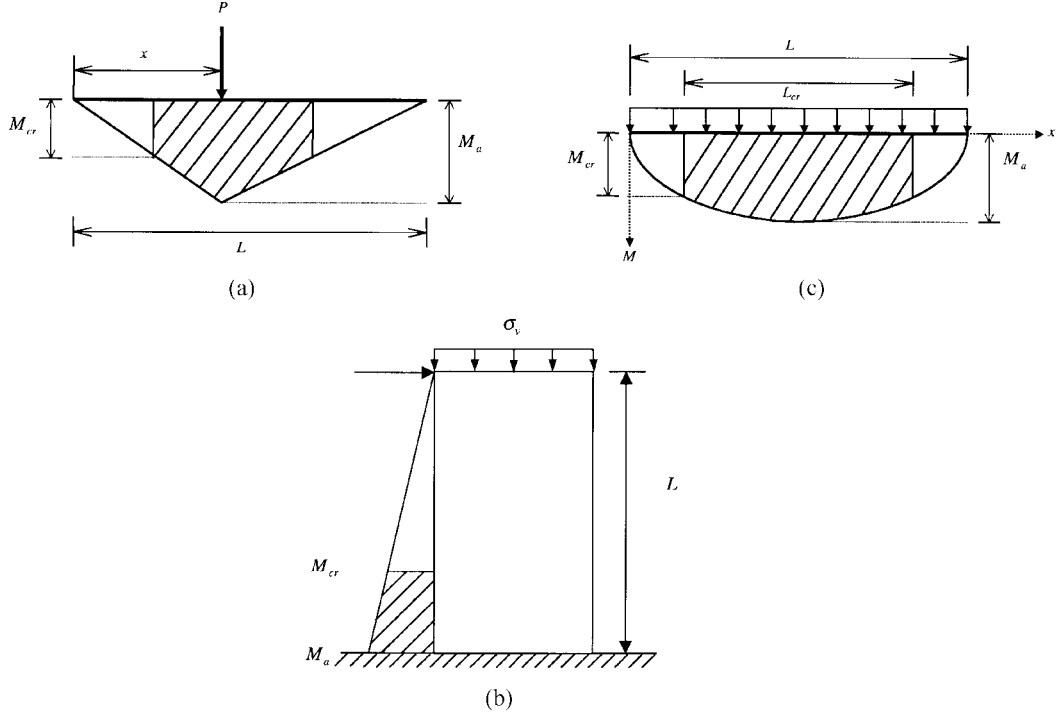


Fig 2 (a) Moment diagram of single-point load, (b) Moment diagram of shear wall with both lateral and vertical loads, (c) Moment diagram of uniformly distributed load

Since a cracked section is associated with cracked moment of inertia I_{cr} while an uncracked section is with uncracked moment of inertia I_{uncr} , the expected value of moment of inertia, for the flexural member, so called effective moment of inertia, can then be expressed as

$$I_e = P_{uncr} I_{uncr} + P_{cr} I_{cr} = (1 - P_{cr}) I_{uncr} + P_{cr} I_{cr} \quad (10)$$

2.2 Derivation of P_{cr} for the mid-point concentrated loading case

For the single-point loading case, the moment diagram is illustrated in Fig. 2(a).

$$S = \frac{1}{2} M_a L$$

$$S_{cr} = \int_{\text{cracked region}} M(x) dx = \frac{L}{2} \left[\frac{M_a^2 - M_{cr}^2}{M_a} \right]$$

Therefore,

$$P_{cr} = \frac{S_{cr}}{S} = \left[1 - \left(\frac{M_{cr}}{M_a} \right)^2 \right] \quad (11)$$

This value is constant for any position of the concentrated load on the flexural member. Eq. (11) has an identical form to the interpolation function of the CEB-FIP code relationship with $\beta=1.0$.

When Eq. (11) is substituted into Eq. (10), a similar expression to the ACI code is achieved when the value of the power m is changed from 3 to 2.

2.3 Derivation of P_{cr} for a cantilever wall with a lateral concentrated load

The moment diagram for this case is shown in Fig. 2(b) (Mickleborough *et al.* 1999). The value of S and S_{cr} can be calculated from simple geometry.

$$S = \frac{1}{2} M_a L$$

and

$$S_{cr} = \int_{\text{cracked region}} M(x) dx = \frac{L}{2} \left[\frac{M_a^2 - M_{cr}^2}{M_a} \right].$$

Therefore,

$$P_{cr} = \frac{S_{cr}}{S} = \left[1 - \left(\frac{M_{cr}}{M_a} \right)^2 \right]. \quad (12)$$

The cantilever wall, with a lateral load acting at the top, has the identical probability formula of cracking occurrence as the simply supported beam with a concentrated load. The probability of cracking occurrence is reduced by the vertical compression load on the top of the wall through increasing the value of M_{cr} shown by Eq. (6). It is not, however, influenced by the height to width ratios of the shear wall since the proposed method predicts the flexural stiffness reduction of shear walls.

2.3 Derivation of P_{cr} for uniformly distributed loading cases

For the uniformly distributed loading case, the moment diagram is shown in Fig. 2(c). The moment diagram can be described by

$$M = \frac{4M_a}{L^2} (Lx - x^2).$$

S and S_{cr} can be obtained as follows,

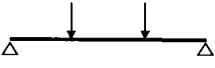
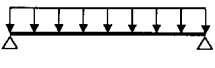
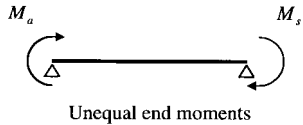
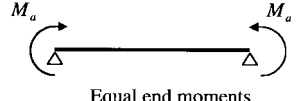
$$S = \int_0^L \frac{4M_a}{L^2} (Lx - x^2) dx = \frac{2}{3} M_a L$$

and

$$S_{cr} = \int_{\frac{L-L_{cr}}{2}}^{\frac{L+L_{cr}}{2}} \frac{4M_a}{L^2} (Lx - x^2) dx = M_a L_{cr} \left[1 - \frac{1}{3} \left(\frac{L_{cr}}{L} \right)^2 \right]$$

From the geometry of the parabolic moment diagram,

Table 1 P_{cr} for various loading cases

Loading case	P_{cr}
 Single point load	$\left[1 - \left(\frac{M_{cr}}{M_a}\right)^2\right]$
 Two point load	$\left[1 - \frac{1}{2}\left(\frac{M_{cr}}{M_a}\right)^2\right]$
 Three point load	$\frac{8}{5}\left[1 - \left(\frac{M_{cr}}{M_a}\right)^2\right]; \frac{3}{4}M_a \leq M_{cr} \leq M_a$ $\left[1 - \frac{8}{15}\left(\frac{M_{cr}}{M_a}\right)^2\right]; M_{cr} \leq \frac{3}{4}M_a$
 Uniform load	$\sqrt{1 - \frac{M_{cr}}{M_a}} \left[1 + \frac{1}{2}\left(\frac{M_{cr}}{M_a}\right)\right]$
 Unequal end moments	$\left[1 / \left(1 + \left(\frac{M_s}{M_a}\right)\right)\right] \left[1 - \left(\frac{M_{cr}}{M_a}\right)^2\right]; M_s \leq M_{cr} \leq M_a$ $\left[1 - \frac{2M_{cr}^2}{M_a^2 + M_s^2}\right]; M_{cr} \leq M_s$ or $\left[1 - \left(\frac{M_{cr}}{M_a}\right)^2\right], M_s = M_a$
 Equal end moments	1, $M_a \geq M_{cr}$

$$\frac{M_{cr}}{M_a} = 1 - \left(\frac{L_{cr}}{L}\right)^2$$

$$P_{cr} = \frac{S_{cr}}{S} = \sqrt{1 - \frac{M_{cr}}{M_a}} \left[1 + \frac{1}{2}\left(\frac{M_{cr}}{M_a}\right)\right]. \quad (13)$$

As the ratio $\frac{M_{cr}}{M_a} \Rightarrow 0$

$$\sqrt{1 - \frac{M_{cr}}{M_a}} = 1 - \frac{1}{2}\left(\frac{M_{cr}}{M_a}\right).$$

Therefore,

$$P_{cr} \left(\frac{M_{cr}}{M_a}\right)_{\rightarrow 0} = \left[1 - \frac{1}{4}\left(\frac{M_{cr}}{M_a}\right)^2\right]. \quad (14)$$

Table 1 presents values of P_{cr} for various loading cases with $M_a \geq M_{cr}$. Various interpolation functions are represented in Fig. 3. This figure indicates that the interpolation function of the uniformly loaded case is very close to that of the two-point loading case, which has the identical form as that of CEB-FIP relationship with $\beta=0.5$. The single point loading condition produces a

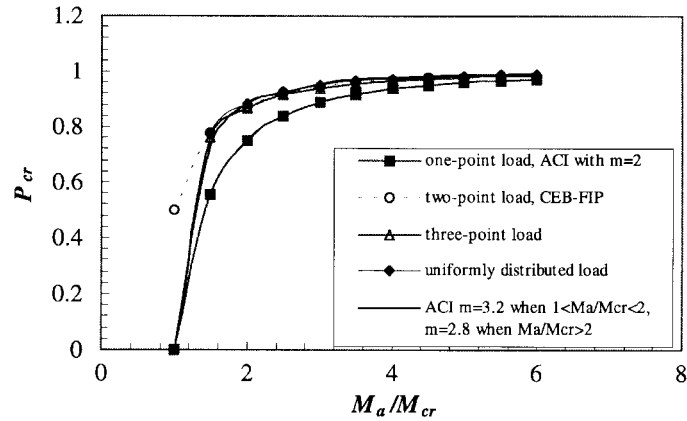


Fig. 3 Theoretical Variation of P_{cr} with the level and type of load

function with the greatest variance from the remainder of the indicated conditions and this function has a similar form to the ACI relationship when m is taken equal to 2. Furthermore the ACI code relationship agrees very well with the three-point and uniformly distributed load with $m=3.2$ when $1 \leq M_a/M_{cr} \leq 2$, and a value of $m=2.8$ when $M_a/M_{cr} > 2$. The discussion above indicates that the proposed method can distinguish the difference between the various load patterns by consideration of the probability of cracking occurrence. It also shows that the CEB-FIP code formula is only applicable in the two-point loading case, while the ACI code relationship is workable in the three-point and uniformly distributed loading cases.

3. Validation of beam tests

3.1 Beam and material details

Three reinforced concrete test beams, with dimensions 300×450 mm cross section and 3460 mm length, were fabricated and used to investigate the reduction of stiffness and the deflection behavior. These specimens were categorized into 3 cases; namely the mid-point concentrated loading test, two-point concentrated loading test, and the uniformly distributed loading test. All test beams were simply supported with an effective span of 3000 mm and with 3-25 mm dia. tensile reinforcement. The compression reinforcement was similar for all test samples using 2-12 mm dia. reinforcement. Ready-mixed commercial concrete was used with ordinary portland cement and a maximum aggregate size of 20 mm. Mix proportions were 1 : 2 : 2.9 with a water-cement ratio of 0.52 and the strength of concrete were 27, 30 and 32 MPa for mid, two-point loading and uniformly distributed loading test. The yield strength of the steel in tension was 460 MPa and an elastic modulus of 200×10^3 MPa. All beams were cast and cured in a similar manner.

3.2 Loading and instrumentation details of beam test

The loading device used for the testing of beams was a 2500 kN DARTEC structural testing system with the application of loading increments between 5 and 20 kN. The deflections of the

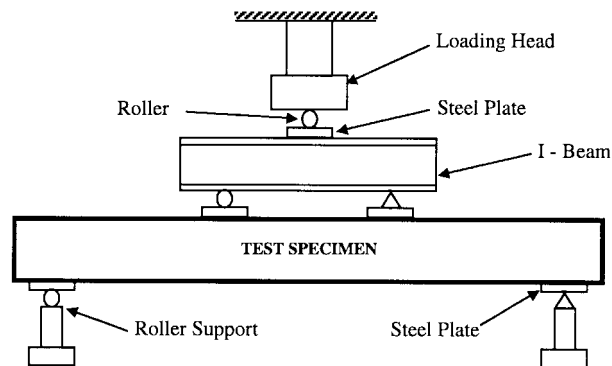


Fig. 4 Typical experimental setup of beam

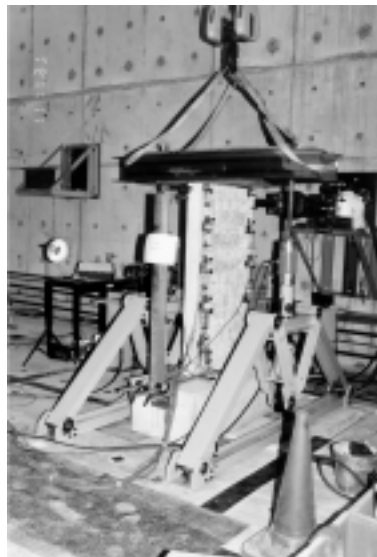


Fig. 5 Setup of SH-H test and detail arrangement of LVDT

beams were measured by dial gauges as well as with linear voltage displacement transducers (LVDT). Five sets of demec points were located along the centre-line of the beam surface to measure the strains and then convert to experimental curvatures at the mid-span of the beam. Fig. 4 illustrates a typical test set-up (Ning *et al.* 1996).

3.3 Comparison between the beam test results and analysis

Each test is reported in the form of **B25-x**, where *x* represents the form of loading, namely; **1** for single-point load, **2** for two-point loading and **U** for the equivalent of uniform loading across the beam.

In the investigation of the flexural behavior of the members, the measured curvature test data has been used to determine the effective moment of inertia. Fig. 6 presents the comparisons of the experimentally determined effective moment of inertia for three beams with 25 mm diameter tensile

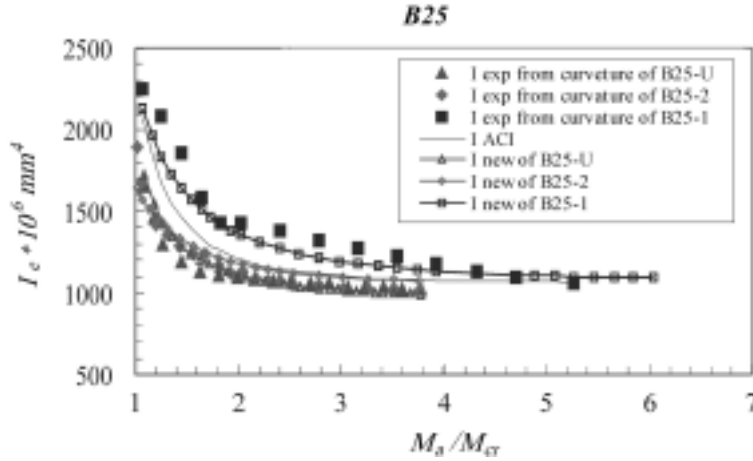


Fig. 6 Comparisons of the experimentally determined I_e for B25 beams subjected to the three loading conditions

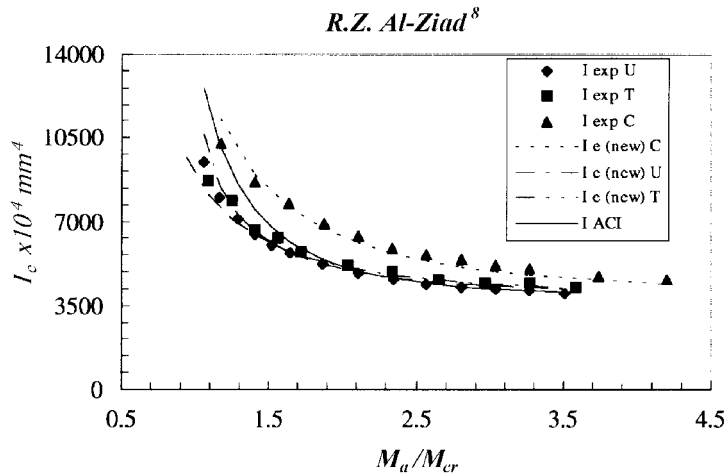


Fig. 7 Comparisons of the proposed model for I_e with beams (R. Z. Al-Zaid) tested under three loading cases

reinforcement subjected to the three loading conditions of mid-point concentrated load, two-point concentrated load and uniformly distributed load. Also indicated in the figure is the variation of I_e from the proposed model, and the ACI prediction at different moment levels. The results clearly indicate that different forms of loading generate different values of I_e , implying a different reduction in stiffness for each beam. The value of I_e obtained for the mid-point loading case is much larger than the other two forms of loading for the same M_u/M_{cr} values. The ACI code relationship always tends to predict the reduction of stiffness is independent of the loading types, hence underestimating I_e for the one-point load case but overestimating I_e for the other two cases considered. The ACI method does not appear to be valid for predicting the stiffness reduction of beams subjected to other load cases. This proposed model gives a more accurate and a more rational approach than the ACI relationship, leading to the conclusion that the interpolation function of stiffness reduction should vary in forms according to the loading type.

3.4 Comparison with previous beam test results

Comparisons of the proposed model for I_e are made from the results of six beams tested by R. Z. Al-Zaid (1991) under mid-point concentrated loads, two-point concentrated loads and uniformly distributed loads respectively. The variations of effective moment of inertia are presented in Fig. 7. This comparison indicates a good correlation between the proposed model and the applicability for different types of the loads while the ACI curve only gives invariable degradation of stiffness of beams for all loading cases.

4. Validation of shear wall tests

4.1 Wall details

Totally, six reinforced concrete structural walls were constructed with three different height-to-width ratios. Type **SH** consisted of two shear walls with dimensions 750 mm wide, 1500 mm high and 125 mm thick, their height-to-width ratio was 2 and these walls are designed to have 300 kN and 500 kN of vertical loading which were designated as **SH-L** and **SH-H** respectively. Type **SM** was 750 mm wide, 1125 mm high and 125 mm thick with height to width ratio of 1.5. **SM-L** and

Table 2 Beam detail and material properties

Batch No.	Beam Type	Specimen geometry				Main steel			Shear steel		Cylinder strength f'_c MPa
		Span	Depth	Effective depth	Width	Steel (b)	Steel (t)	Ratio%	Type	Spacing	
1	B25-1	3000	450	393.5	300	3T25	2C12	1.08	R12	100	27
2	B25-2	3000	450	393.5	300	3T25	2C12	1.08	R12	100	30
3	B25-U	3000	450	393.5	300	3T25	2C12	1.08	R12	100	32

All dimensions are millimetres:
(t): top steel; (b): bottom steel

Table 3 Shear wall detail and material properties

Mark	H_w/l_w	Materials and section properties (concrete)			Loading	
		I_{cr} 10^6 mm ⁴	Young's modulus E MPa	Cylinder strength f'_c MPa	Applied axial load F_v kN	Actual stress MPa
SH-L	2	1062	23789	45	357	3.8
SH-H	2	906	28991	56	493	5.3
SM-L	1.5	1230	19769	30	334	3.6
SM-H	1.5	795	30629	57	486	5.2
SL-L	1	795	30629	57	360	3.8
SL-H	1	1230	19769	30	477	5.1

$$\rho_{ver}\% = 1.17$$

$$\rho_{hor}\% = 0.39$$

SM-H are designated for the loading conditions as previously noted. Type **SL** walls were 750 mm wide, 750 mm high and 125 mm thick, their height to width ratio is 1 and are designated as **SL-L** and **SL-H** according to the two loading cases. In all shear wall structures, the walls were monolithically connected to foundation beams. The dimension of the foundation were 1400 mm long, 600 mm wide and 400 mm deep, and were designed to bolt the shear walls to the laboratory test floor, simulating a rigid foundation without cracking during the range of test loading.

Since the main variables examined were the level of constant vertical load and height to width ratio, the percentage of vertical and horizontal reinforcement in the all the shear walls was kept constant throughout the experimental program. For all wall structures, uniformly distributed horizontal reinforcement of 14-10 mm dia. @110 mm centers, ($\rho_{hor}=0.39\%$), and vertical reinforcement of 6 mm dia. @100 mm centers, ($\rho_{ver}=1.17\%$), were placed in the 125 mm thick web. The vertical and horizontal reinforcement of the walls comprised high tensile deformed steel bars of 10 and 6 mm diameter, respectively. Details of concrete properties are presented in Table 3. Although the commercial concrete used in all specimens was to be supplied with the same mix design with 30 MPa strength of concrete, the strength of concrete of each specimen determined on the day of testing of the shear walls varied significantly from 28 MPa to 57 MPa.

4.2 Load and instrumentation details of wall test

A large lateral hydraulic actuator (DARTEC) with 400 kN capacity was installed on the laboratory reaction wall. A mechanism was designed and fabricated that effectively eliminated restraint by the vertical loading devices called a gravity-load simulator. The simulator was designed with reference to Yarimci *et al.* (1967). The device approximates true gravity load when it is used together with a tension-loading system. The load line of this system functions such that when the sideways is between 0 mm and 200 mm, the load remains vertical and moves with the sideways of the structure. For shear wall tests the actual lateral deflections were always generally less than 20 mm, hence no horizontal component of vertical load was induced. After the total constant vertical force was applied, the wall specimen was incrementally loaded with the horizontal (lateral) load at a rate of approximately 0.02 kN/sec until failure.

The top lateral deflection was measured by a linear voltage displacement transducer (LVDT). LVDTs were used to measure the curvatures along the height of shear walls in order to obtain the flexural deflection. For **SH** cases 10 LVDTs were positioned on both extreme side of shear walls with five level evenly spaced as shown in Fig. 5. For **SM** cases 8 LVDTs were used and 4 LVDTs for **SL** cases.

4.3 Data retrieval of wall tests

The experimental test data from the applied loading, deflections and strain gauge measurements were recorded by DATA LOG system. The resolution of LVDTs and loading system were 0.01 mm and 0.01 kN respectively. During the reading cycle, readings were taken from all the measurement devices and recorded at intervals of 5 seconds (Ning 1998).

4.4 Comparison between the shear wall test results and analysis

The focus of this work was placed on consideration of the reduction of flexural stiffness of

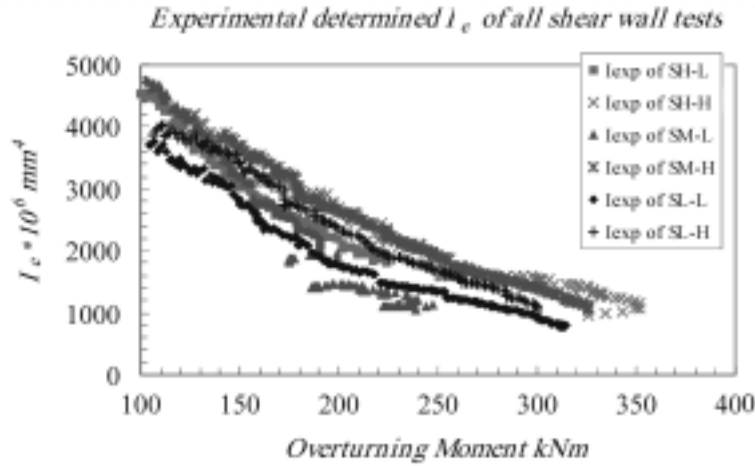


Fig. 8 Experimental determined I_e of all shear wall tests

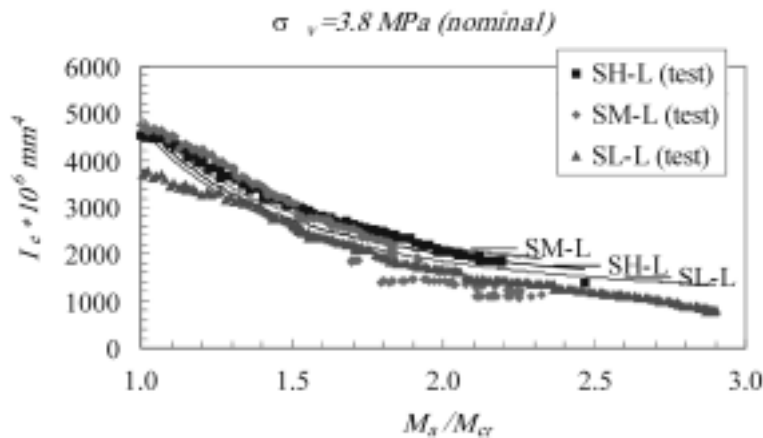


Fig. 9 Stiffness comparisons between analytical and test results of shear walls under vertical stress $\sigma_v=3.8$ MPa

reinforced concrete shear wall due to cracking, with the increasing lateral load. The experimental curvature data were used to determine the test values of flexural stiffness. Fig. 8 presents the flexural stiffness reduction of all shear walls as a function of the increasing overturning moment from the application of the lateral load. It is shown that the increase in the vertical compression loads result in larger cracked moment, M_{cr} , larger ultimate overturning moment and a lower rate of flexural stiffness reduction than the structure with the lower vertical compression loads. Within the range of structural height to width ratios tested, only a minor influence is noted on the rate of flexural stiffness degradation. The ultimate overturning moments of the shear walls increase with decreasing height to width ratios. Figs. 9 and 10, indicate the comparisons of flexural stiffness reduction between the experimentally determined values and analytical predicted ones under two vertical loading cases. These results give very good agreements between the analytically (Eq. 10-12) and experimentally determined reduction of flexural stiffness of reinforced concrete shear walls. Moreover, from Fig. 11 most calculated to experimentally determined ratios of flexural stiffness are

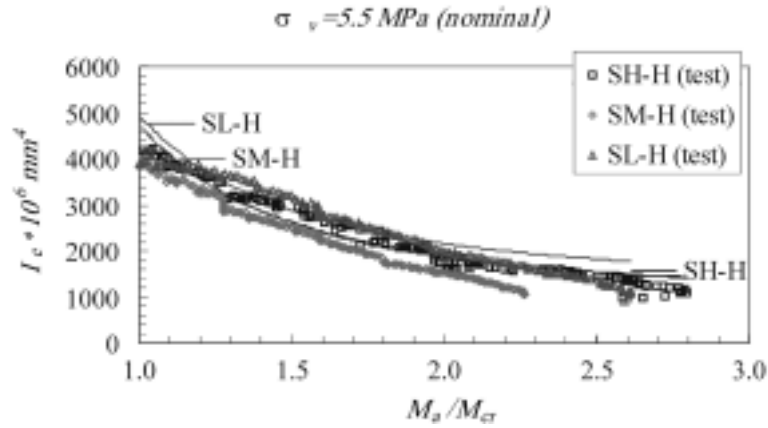


Fig. 10 Stiffness comparisons between analytical and test results of shear walls under vertical stress $\sigma_v=5.6$ MPa

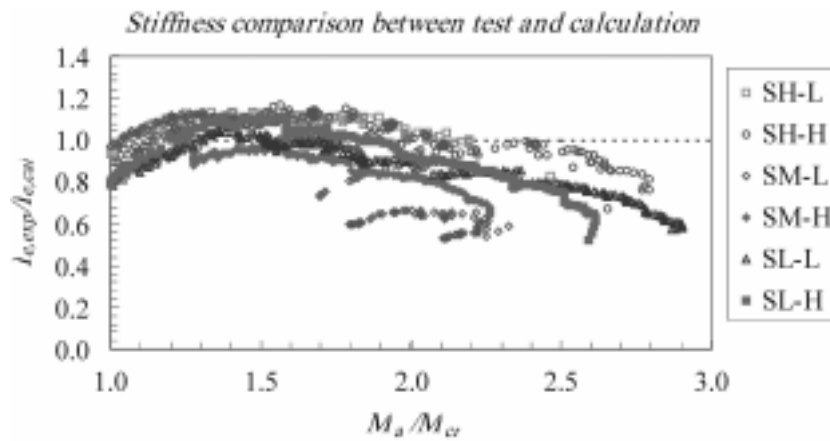


Fig. 11 I_{exp}/I_{cal} versus M_a/M_{cr}

distributed within the range of 0.84 to 1.16, with the idealized value of 1 occurring when M_a/M_{cr} is smaller than about 2.5. All the results verify that Eq. (8) provides a good evaluation of the probability of cracking occurrence which is combined with Eq. (10) to produce an accurate expected mean value of flexural stiffness within the working load range of structural behavior.

5. Conclusions

A probability-based analytical model to provide improved accuracy over conventional methods for the prediction of effective stiffness of reinforced flexural members, under service load conditions, has been developed.

- (1) The model physically relates the I_e to an expression mathematically equivalent to the probability of the cracking occurrence. This probability is equal to, the ratio of the area of the moment

diagram over which the working moment exceeds the cracking moment, S_{cr} , to the total area of moment diagram, S . The relationship can be derived from the shape and magnitude of the moment diagram for any conditions of loading.

- (2) The CEB-FIP relationship can be applied to the mid-point loading case with coefficient $\beta=1$, two-point loading case with coefficient $\beta=1/2$ and can also be used for the uniformly distributed loading case with $\beta=1/4$ as a good approximation. When using the ACI relationship, the effective I_e due to a one-point concentrated load is always underestimated, and that due to a two-point load or uniformly distributed load is overestimated.

An experimental beam testing program, together with other published works, indicates good agreement with the proposed model for reinforced concrete beams under varying types of loading.

Experimental tests on shear walls subjected to combinations of both lateral and vertical gravity loads show the proposed method can provide an accurate prediction of the flexural stiffness reduction for walls with various width to height ratios.

Acknowledgements

This work was supported by the Research Grants Council of Hong Kong under project No. HKUST-543/94E, and was based upon research conducted by Feng Ning under the supervision of Neil Mickleborough and Chun-Man Chan for the Degree of Doctor of Philosophy in the Department of Civil Engineering at the Hong Kong University of Science & Technology, Hong Kong.

References

- American Concrete Institute, (1995), "*Building code requirements for reinforced concrete (ACI 318-83)*," ACI Committee 318, Detroit, 111pp.
- Al-Shaikh, Abdulrahman, H., and Al-Zaid, Rajeh Z. (1993), "Effect of reinforcement ratio on the effective moment of inertia of reinforced concrete beams," *ACI Struct. J.*, Mar.-Apr., **90**(2), 144-149.
- Al-Zaid, Rajeh Z., Al-Shaikh, Abdulrahman, H., and Abu-Hussein, Mustafa, M. (1991), "Effect of loading type on the effective moment of inertia of reinforced concrete beams," *ACI Struct. J.*, Mar.-Apr., **88**(2), 184-190.
- Branson, D.E. (1977), *Deformation of Concrete Structures*, McGraw-Hill, New York.
- (CEB-FIP) (1978), "*Model code for concrete structures (MC-78)*," Comite Euro-International du Beton-Federation Internationale de la Precontrainte Lausanne.
- Canadian Standards Association (1984), *Design of Concrete Structures for Buildings (CAN3-A23.3-M84)*. Rexdale, 281pp.
- Ghali, A. (1993), "Deflection of reinforced concrete members: A critical review," *ACI Struct. J.*, **90**(4), 364-373, Jul.-Aug.
- Mickleborough, N.C., Ning, F., and Chan, C-M. (1999), "Prediction of the stiffness of reinforced concrete shear walls under service loads", *ACI Struct. J.*, **96**, No., Nov. Dec.
- Murashev, V.E. (1940), *Theory of Appearance and Opening of Cracks, Computation of Rigidity of Reinforced Concrete Members*, Stroitel'naya Promishlennost (Moscow), 11.
- Ning, F., Mickleborough, N.C., and Chan, C.M. (1998), "Reinforced concrete shear walls: Serviceability prediction," Technical Report No. ST98/1, Department of Civil & Structural Engineering, The Hong Kong University of Science and Technology.
- Ning, F., Mickleborough, N.C., and Chan, C.M. (1996), "Reinforced concrete members: Serviceability prediction," Technical Report No. ST96/1, Department of Civil & Structural Engineering, The Hong Kong

University of Science and Technology.
Standards Association of Australia (1982), *SAA Concrete Structures Code (AS 1480-1982)*, Sydney.
Yarimci, E., Yura, J.A., and Lu, L.W. (1967), "Techniques for testing structures permitted to sway," *Experimental Mechanics*, **7**(8).